

## 1 **Supplementary Online Information (SOM)**

### 3 **Title: High concentrations of biological aerosol particles and ice nuclei during and** 4 **after rain**

5 **Authors:** J. A. Huffman<sup>1\*</sup>, C. Pöhlker<sup>2</sup>, A. J. Prenni<sup>3\*</sup>, P. J. DeMott<sup>3</sup>, R. H. Mason<sup>4</sup>, N. H.  
6 Robinson<sup>5</sup>, J. Fröhlich-Nowoisky<sup>2</sup>, Y. Tobo<sup>3</sup>, V. R. Després<sup>6</sup>, E. Garcia<sup>3</sup>, D. J. Gochis<sup>7</sup>, E.  
7 Harris<sup>2</sup>, I. Müller-Germann<sup>2</sup>, C. Ruzene<sup>2</sup>, B. Schmer<sup>2</sup>, B. Sinha<sup>2,8</sup>, D. A. Day<sup>9</sup>, M. O. Andreae<sup>2</sup>,  
8 J. L. Jimenez<sup>9</sup>, M. Gallagher<sup>5</sup>, S. M. Kreidenweis<sup>3</sup>, A. K. Bertram<sup>4\*</sup>, U. Pöschl<sup>2\*</sup>

### 9 **Affiliations:**

10 <sup>1</sup>Department of Chemistry & Biochemistry, University of Denver, 2190 E. Illif Ave., Denver,  
11 CO, 80208, USA.

12 <sup>2</sup>Max Planck Institute for Chemistry, Hahn-Meitner-Weg 1, D-55128, Mainz, Germany.

13 <sup>3</sup>Department of Atmospheric Sciences, Colorado State University, 1371 Campus Delivery, Fort  
14 Collins, CO, 80523, USA.

15 <sup>4</sup>Department of Chemistry, University of British Columbia, Room D223, 2036 Main Mall,  
16 Vancouver, BC, V6T1Z1, Canada.

17 <sup>5</sup>Centre for Atmospheric Sciences, University of Manchester, Simon Building, Oxford Road,  
18 Manchester, M139PL, UK.

19 <sup>6</sup>Institute for General Botany, Johannes Gutenberg University, Müllerweg 6, D-55099, Mainz,  
20 Germany.

21 <sup>7</sup>National Center for Atmospheric Research, PO Box 3000, Boulder, CO, 80307, USA.

22 <sup>8</sup>IISER Mohali, Department of Earth and Environmental Science, Sector 81, S. A. S. Nagar,  
23 Manauli PO, 140306, India.

24 <sup>9</sup>Cooperative Institute for Research in the Environmental Sciences and Department of Chemistry  
25 and Biochemistry, University of Colorado, Boulder, CO USA.

26 \* Correspondence to: alex.huffman@du.edu (J. A. H.); anthony.prenni@colostate.edu (A. J. P.);  
27 bertram@chem.ubc.ca (A. K. B.); u.poschl@mpic.de (U. P.)  
28

## 29 **Supplementary Materials:**

30 S1 Materials and Methods

31 Figures S1-S3

32

### 33 **S1 Materials and Methods**

#### 34 ***S1.1 Site and Campaign Description***

35 The BEACHON-RoMBAS (Bio-hydro-atmosphere interactions of Energy, Aerosols, Carbon,  
36 H<sub>2</sub>O, Organics and Nitrogen – Rocky Mountain Biogenic Aerosol Study) campaign was a  
37 component of the greater BEACHON project sponsored by the National Center for Atmospheric  
38 Research (<http://cires.colorado.edu/jimenez-group/wiki/index.php/BEACHON-RoMBAS>;  
39 <http://web3.acd.ucar.edu/beachon/>). BEACHON-RoMBAS brought together a large,  
40 interdisciplinary set of scientists to address issues surrounding the biogeochemical cycling of  
41 carbon and water at a location representative of the semi-arid Western U.S. The measurements  
42 were located in a part of the Manitou Experimental Forest in a semi-arid, montane ponderosa  
43 pine zone in the Central Rocky Mountains 35 km northwest of Colorado Springs, Colorado and  
44 15 km north of Woodland Park, CO (2370 m elevation, lat. 39°6'0" N, long. 105°5'30" W). All  
45 instruments and samplers were sampled from a height of 1 – 4 m above ground from fixed inlets,  
46 with the exception of the WIBS, high-volume sampler, and biosamplers (details listed below).

47

#### 48 ***S1.2 Meteorological and Leaf Moisture Measurements***

49 Precipitation occurrence, rate and microphysical state (i.e., rain versus hail) were measured using  
50 a laser-optical disdrometer (PARTicle Size and VELOCITY ‘PARSIVEL’ sensor; OTT Hydromet  
51 GmbH, Kempton, Germany). The instrument senses a falling hydrometeor by measuring the  
52 magnitude and duration of attenuation of a temporally continuous 2-dimensional laser beam (780

53 nm) through which the hydrometeor passes. It, therefore, directly detects the presence of falling  
54 hydrometeors without the time delay of typical tipping bucket gauges and with greater particle  
55 size sensitivity than typical weighing gauges. Particle size is estimated from the magnitude of  
56 beam attenuation. Particle fall speed is determined from the duration of beam attenuation while  
57 overall precipitation rate and microphysical classification estimates are generated from a  
58 combination of the size and fall speed measurements. The sensor detects liquid hydrometeor  
59 particles ranging in size from 0.2 to 5 mm in diameter, solid hydrometeors ranging in size from  
60 0.2 to 25 mm and provides estimates of particle velocities from 0.2 to 20 m/s. The stated  
61 accuracy of liquid precipitation rate estimates is +/- 5%. Only the rainfall rate (mm/hr) is  
62 discussed in this text.

63  
64 Leaf wetness state was characterized using a dielectric Leaf Wetness Sensor (LWS; Decagon  
65 Devices, Inc.). The sensor detects and provides a relative measure of the water or ice content on  
66 or near the sensor surface (within ~1 cm) by measuring the dielectric constant of the surface. The  
67 sensor outputs a voltage (measured in millivolts, mV) which is directly proportional to the  
68 amount of water or ice in or near the sensor upper surface. Attribution of the cause of wetness  
69 due to rain or dew formation (i.e. local condensation) is determined by comparing LWS voltage  
70 with optical precipitation measurements and by the pattern of voltage readings from the sensor.  
71 Sharp increases in the mV signal that are concurrent with precipitation events are characterized  
72 as ‘rainfall wetness’ while slowly increasing mV values that are unaccompanied with  
73 precipitation events are characterized as dew formation.

74

75 Other meteorological parameters such as barometric pressure, air temperature, humidity and  
76 wind speed and direction were measured using a WXT520 Weather Transmitter (Vaisala, Inc.,  
77 Helsinki, Finland). The weather transmitter, the disdrometer and the LWS were all located at the  
78 Manitou Experimental Forest observatory within 100 m of the rest of the particle measurements  
79 described below.

80

### 81 ***SI.3 UV-APS***

82 An ultraviolet aerodynamic particle sizer (UV-APS; TSI Inc. Model 3314, St. Paul, MN) was  
83 utilized for this study following the procedure described by Huffman et al. (Huffman et al.,  
84 2010). Aerodynamic particle diameter ( $D_a$ ) is provided in the range of 0.54 – 19.81  $\mu\text{m}$  by  
85 measuring the time of flight between two continuous-wave red (633 nm) He-Ne lasers. Total  
86 fluorescence of aerosol particles (non-wavelength-dispersed) in the wavelength range of 420 –  
87 575 nm is detected after pulsed excitation by an Nd:YAG laser ( $\lambda_{\text{ex}} = 355 \text{ nm}$ ). UV-APS number  
88 concentrations are reported here as integrated between 1 – 20  $\mu\text{m}$ . Smaller particles are  
89 transmitted within the instrument less efficiently and thus should be considered as lower limit  
90 values. Aerosol sampling was performed with a volumetric flow of 5  $\text{L}\cdot\text{min}^{-1}$  (LPM) at ambient  
91 pressure and temperature, split within the instrument into a sample flow of  $1.0 \pm 0.1$  LPM and a  
92 sheath flow of  $4.0 \pm 0.1$  LPM (pressure difference feedback control). The instrument was  
93 controlled and the measurement data were recorded with an external computer connected via  
94 serial port using the manufacturer's Aerosol Instrument Manager software (TSI AIM).  
95 Measurements were initiated every 5 minutes and integrated over a sample length of 285 s. Five-  
96 minute sample measurements were continuously repeated over a period of five weeks from 20  
97 July to 23 August, 2011 (35 days) and only briefly interrupted for maintenance procedures

98 (usually less than 30 minutes per week). The local time (LT) used for data analysis and plotting  
99 refers to Mountain Daylight Time (MDT). All times reported here are listed as LT.

100

101 Fluorescent particles ( $N_f$ ) detected by the UV-APS can be regarded as a lower limit for the  
102 abundance of primary biological aerosol particles (Huffman et al., 2010; Pöhlker et al., 2012),  
103 utilizing nicotinamide adenine dinucleotide (NADH) and riboflavin as dominant biological  
104 fluorophores. The UV-APS instrument sampled air from a 0.75 inch laminar flow inlet from ~4  
105 m above ground into a climate-controlled trailer at ground level.

106

#### 107 ***SI.4 WIBS***

108 The waveband integrated bioaerosol sensor – model 4 (WIBS4; University of Hertfordshire) is a  
109 dual channel single particle fluorescence spectrometer (Kaye et al., 2005; Foot et al., 2008;  
110 Gabey et al., 2010). Upon detection of a particle, xenon lamps provide two consecutive pulses of  
111 light at 280 nm and 370 nm, in order to stimulate fluorescence of the tryptophan and NADH  
112 biofluorophores respectively. The fluorescence of a particle is measured between 310-400 nm  
113 (the FL1 channel) and 400-600 nm (the FL2 channel), capturing tryptophan fluorescence, and  
114 400-600 nm, capturing NADH fluorescence. This leads to three separate fluorescence channels:  
115 FL1\_280, FL2\_280 and FL2\_370. The forward scattering signal of the particle is also measured  
116 at four angular offsets using a quadrant photo-multiplier tube. This allows for measurements of  
117 size and asymmetry. The WIBS4 model is essentially the same as the WIBS3 model employed  
118 by Gabey et al. (2010), but with improved optics and electronics providing a more precise signal.  
119 Baseline fluorescence is recorded by regularly measuring the internal fluorescence of the  
120 instrument when no particles are present. The increased precision of the model 4 WIBS allows

121 for the detection of more marginally fluorescent particles than was possible using previous  
122 WIBS models.

123  
124 The WIBS4 was located on an automated profiling system running up the main measurement  
125 tower, which allowed profile measurements to be made between 3 m and 22 m. Profiles  
126 consisted of an eight stage profile up, lasting around 45 minutes, and a corresponding continuous  
127 profile down, lasting about 3 minutes. The WIBS4 total particle size distribution compared well  
128 with a co-sampling Grimm OPC, particularly in the super-micron regime. A subset of the WIBS4  
129 single particle data (8000 particles) was analyzed using hierarchical agglomerative cluster  
130 analysis using a group average distance metric. This clustering was analyzed in five dimensions  
131 which were z-score normalized before analysis: the three fluorescence channels, size, and  
132 asymmetry. A suitable solution was assessed by inspecting the coefficient of determination and  
133 the root mean squared distance between clusters for each (e.g. Robinson et al., 2011).  
134 Concentration time series for each cluster were established by comparing each of the remaining  
135 particles to the centroid of each cluster. Each time series was apportioned a fraction of the  
136 particles' count which was inversely proportional to the distance of the particle from each cluster  
137 centroid (expressed in number of standard deviations of the centroid).

138  
139 Bioaerosol fluxes were estimated for each cluster by combining the concentration gradient with  
140 vertical wind speed data using:

141

142 Equation S1 
$$F = -0.16 \left( \frac{\Delta z_u \Delta u}{\left( \ln \frac{z_{u2}}{z_{u1}} \right)^2} \right) \left( \frac{\Delta c}{\Delta z_c} \right)$$

143  
144  
145  
146  
147  
148  
149  
150  
151  
152  
153  
154  
155  
156  
157  
158  
159  
160  
161  
162  
163  
164  
165

Where  $\Delta u$  is the difference between vertical wind speed measurements measured at heights  $z_{u1}$  and  $z_{u2}$  which are  $\Delta z_u$  apart, and  $\Delta c$  is the difference in concentrations between two heights which are  $\Delta z_c$  apart (Lindemann et al., 1982).

## ***S1.5 Filter and Impactor Aerosol Samples***

### ***S1.5.1 Sample Collection***

#### ***S1.5.1.1 Cascade Aerosol Impactor (MOUDI)***

Size-resolved particle samples were collected using a micro-orifice uniform deposition impactor (MOUDI; MSP model 110-R) at a flow-rate of 30 LPM via a dedicated inlet. Samples used for offline ice nucleation analysis were collected onto hydrophobic, siliconized glass slides (Hampton Research, HR3-2125). The MOUDI sampler provided aerosol fractionation according to the following aerodynamic diameter size cuts ( $D_{50}$ ,  $\mu\text{m}$ ) (Marple et al., 1991):

Stage 1	18.0
Stage 2	10.0
Stage 3	5.6
Stage 4	3.2
Stage 5	1.8
Stage 6	1.0
Stage 7	0.56
Stage 8	0.32
Stage 9	0.18
Stage 10	0.10

167 Stage 1 is typically referred to as the pre-impactor, and stages 2-11 refer to stages in the MOUDI  
 168 impactor. Because we are interested in large particles we refer to the pre-impactor as Stage 1 and  
 169 list all stages as 1-11. Thus, the numbering scheme utilized here is shifted lower by one with  
 170 respect to the common usage for MOUDI samplers.

171  
 172 MOUDI samples collected at the following times were analyzed by fluorescence microscopy and  
 173 used for microscopic ice nucleation activation experiments as discussed in the manuscript:

174	M01 (dry period)	7/22 14:29 – 7/23 09:41	(1152 min.)
175	M10 (rain period)	8/2 05:55 – 8/3 05:55	(1440 min.)
176	M26 (rain period)	8/16 20:26 – 8/17 06:32	(606 min.)
177	M27 (dry period)	8/17 06:35 – 8/17 19:46	(791 min.)

178  
 179 Size distribution of ice nuclei shown in Figure 2C for dry periods are average of samples M1 and  
 180 M27; Figure 2D for rain periods are average of samples M10 and M26. Corresponding time  
 181 periods for UV-APS are identical to MOUDI sample periods.

182  
 183 ***S1.5.1.2 High-volume Sampler***

184 Total aerosol samples for DNA analysis were collected onto 150 mm glass fiber filters  
 185 (Machery-Nagel, Type MN 85/90, 406015) using a self-standing high-volume sampler (Digital  
 186 DHA-80) operated at 1000 LPM and located approximately 50 m from the sampling trailer.  
 187 Filters were pre-baked at 500 °C (12 h) to remove any contaminant DNA and stored in pre-baked  
 188 aluminum bags before and after sampling.

189

190 ***S1.5.1.3 Glass Slide Impactor Samples***

191 Total aerosol samples were collected onto glass cover slides (13 x 13 mm) using a home-built,  
192 single-stage impactor (Flow-rate 1.2 LPM, D<sub>50</sub> cut 0.5 μm). The impactor glass substrates were  
193 coated with a thin layer of high viscosity grease (Baysilone grease, Bayer, Germany) administered  
194 via hexane solution to reduce particle bounce. Single-stage impactor and housing for Nuclepore®  
195 filters (below) sub-sampled from a separate inlet immediately next to MOUDI and UV-APS  
196 inlets.

197

198 Glass slide impactor samples collected at the following times are shown in Figures 2A and 2B  
199 and discussed in the manuscript:

200	G09 (dry period)	7/31 12:17 – 12:49	(32 min.)
201	G21 (rain period)	8/3 23:56 – 8/4 0:27	(31 min.)

202

203 ***S1.5.1.4 Nuclepore® Filters***

204 Aerosol samples for electron microscopy analysis were collected with a stacked filter housing  
205 using 12 mm diameter gold-coated Nuclepore® polycarbonate filters with pore sizes of 2 μm for  
206 coarse particles and 0.2 μm for fine particles, respectively. The volume flow through the stacked  
207 filter unit was nominally 2.0 LPM.

208

209 Stacked filter samples collected at the following times are discussed in the manuscript:

210	S10 (dry period)	7/31 11:57 – 15:58	(241 min.)
211	S12 (dry period)	7/31 19:58 – 23:55	(237 min.)

212	S20 (rain period)	8/4 3:52 – 8:04	(252 min.)
213	S23 (rain period)	8/4 16:23 – 20:24	(261 min.)

214

#### 215 ***S1.5.1.5 Bio-Sampler Impactors***

216 Size-resolved viable bioparticles were collected via two types of impactors directly into growth  
217 media (flow-rate 28 LPM). Andersen cascade impactors (Graseby Andersen; Atlanta, GA)  
218 collect particles onto one of six sequential sample plates designed to collect large particles on  
219 upper plates and smaller particles on lower plates. Slit samplers (New Brunswick Scientific Co.;  
220 Edison, NJ) collect particles without selection due to sizing, but the collection stage rotates such  
221 that particles are deposited in a circular arc to give time resolution of ~2 minutes over the course  
222 of a 60 minute sample time. Samplers were placed ~2 m above ground on a piece of wooden  
223 fencing that allowed air to pass through the support surface above ground and operated at 28  
224 LPM. The surfaces of samplers were sterilized with isopropyl alcohol before each period of  
225 collection to remove contaminant organisms. Samplers were operated separately for optimized  
226 collection of fungi and bacteria. Fungal growth medium (malt extract medium) was prepared by  
227 according to Medelin et al. (Madelin, 1994) with streptomycin (40 units, Sigma Aldrich) and  
228 ampicillin (20 units, Fisher Scientific). Bacterial growth medium (Luria Bertani medium; LB)  
229 was prepared according to Lighthart and Shaffer (Lighthart and Shaffer, 1995) with  
230 cycloheximide (200 µg/mL, Sigma Aldrich). Samples for bacterial analysis were collected for 60  
231 minutes, and samples for fungal analysis were collected for 20 minutes. Collection dishes were  
232 immediately removed from samplers after each use and placed in an incubator (IncuMax,  
233 IC150R) temperature-controlled at 25 °C. Fungal colonies were incubated for ~3 days before  
234 counting and picking into 20 µl of sterile water. Bacterial colonies were incubated for ~7 days

235 before counting and picking into sterile water. The picked colonies were lysed at 95 °C for 10  
236 min.

237

### 238 ***S1.5.2 Fluorescence Microscopy***

239 Fluorescence microscopy images were taken on a BZ-9000 Fluorescence Microscope (Keyence,  
240 Inc., Osaka, Japan). The instrument was equipped with a super high-compression mercury lamp  
241 (120 W) and a 2/3-inch, 1.5 mega pixel monochrome CCD. The following fluorescence filters  
242 were used to take images in different spectral ranges: OP-66834 DAPI-BP ( $\lambda_{\text{ex}}=360/20$  nm,  
243  $\lambda_{\text{Dichroic}}=400$  nm,  $\lambda_{\text{Absorp}}=460/25$  nm), OP-66836 GFP-BP ( $\lambda_{\text{ex}}=470/20$  nm,  $\lambda_{\text{Dichroic}}=495$  nm,  
244  $\lambda_{\text{Absorp}}=535/25$  nm), OP-66838 TexasRed ( $\lambda_{\text{ex}}=560/20$  nm,  $\lambda_{\text{Dichroic}}=595$  nm,  $\lambda_{\text{Absorp}}=630/30$   
245 nm). Filter specifications are represented as wavelength and peak width ( $\lambda/\text{FWHM}$ ).

246

247 In Fig. 2A and 2B an overlay of fluorescent emission from all three fluorescence microscope  
248 channels (DAPI, GFP, TexasRed) onto a brightfield image of the same sample area is shown. For  
249 comparability the exposure times of the individual fluorescence images in Fig. 2A and 2B were  
250 set to the same values. The overlay image Fig. 2B is dominated by “blue-green” fluorescence  
251 indicating strong emissions in the DAPI ( $\lambda_{\text{ex}} = \sim 360$  nm,  $\lambda_{\text{em}} = \sim 460$  nm) and GFP  
252 ( $\lambda_{\text{ex}} = \sim 470$  nm,  $\lambda_{\text{em}} = \sim 535$  nm) channels. Blue-green fluorescence is characteristic for biological  
253 material and mainly originating from protein and coenzyme fluorophores (Pöhlker et al., 2012).  
254 In contrast “red-yellow” fluorescence is predominating in the overlay image in Fig. 2A  
255 indicating strong emission in the TexasRed channel ( $\lambda_{\text{ex}} = \sim 560$  nm,  $\lambda_{\text{em}} = \sim 630$  nm). Red-yellow  
256 fluorescence is regarded to be somewhat characteristic/typical for mineral dust (Bozlee et al.,  
257 2005).

258

### 259 ***S1.5.3 SEM***

260 Scanning electron microscopy (SEM) images of aerosol particles were acquired using the  
261 secondary electron in-lens detector of a high-performance field emission instrument (LEO 1530  
262 FESEM, EHT 10 keV, WD 9 mm). The elemental composition of inorganic components was  
263 characterized using the Oxford Instruments ultra-thin-window energy-dispersive X-ray (EDX)  
264 detector.

265

266 The filter samples were scanned using a semi-automated spot counting technique (Sinha et al.,  
267 2008; Pöschl et al., 2010) at a magnification of  $6500 \times$  (pixel size 88.9 nm) for coarse and  $19500$   
268  $\times$  (pixel size 29.6 nm) for fine particle filters. Particles located on the predefined equidistant  
269 spots of the counting grid were automatically counted, and the recorded data were used to  
270 classify the particles according to size, composition, and mixing state. With spot counting, the  
271 probability for particles of a certain size and type to be counted is directly proportional to the 2-  
272 D surface area of the particles and the fraction of the filter surface covered by such particles.  
273 This relationship is used to upscale the counting results from the investigated filter area to the  
274 total filter area.

275

### 276 ***S1.5.4 DNA Analysis of Aerosol Samples***

277 To determine fungal diversity from the air filter samples (high-volume sampler, S1.5.1.2)  
278 optimized methods of DNA extraction, amplification, and sequence analysis of the internal  
279 transcribed spacer (ITS) regions as described in Fröhlich-Nowoisky et al. (2009; 2012) were  
280 used. In addition to fungi, the primer pair ITS4Oo and ITS5 (Nikolcheva and Bärlocher, 2004)

281 was used for amplification of *Peronosporomycetes* (formerly *Oomycota*). Also specific for this  
282 study, the internal transcribed spacer regions from fungal lysates, obtained from the cultivation  
283 experiments of impactor samples (Anderson Cascade Bio-Sampler Impactors, S1.5.1.5), were  
284 amplified with the primer pair ITS4 and ITS5 (White et al., 1990; Fröhlich-Nowoisky et al.,  
285 2009; Fröhlich-Nowoisky et al., 2012). The obtained PCR products were sequenced using the  
286 primer ITS5 and sequence analysis was performed as described in Fröhlich-Nowoisky et al.  
287 (2009; 2012). The sequences from the obtained operational taxonomic units have been deposited  
288 in the GenBank database under following accession numbers: JX135610 - JX136661 (Fungi) and  
289 JQ976038 - JQ976273 (*Peronosporomycetes*).

290

291 For the determination of bacterial diversity from high-volume aerosol filter samples (see also  
292 S.1.5.1.2) DNA was extracted as described by Després et al. (2007). The 16S ribosomal gene  
293 was first amplified for taxonomic identification with primer pairs 9/27f and 1492r (Weisburg et  
294 al., 1991) with PCRs conditions given by Després et al. (2007), and then cloned and sequenced.  
295 The same primer pair was used for the bacterial lysates obtained from Andersen sampler culture  
296 plates (Anderson Cascade Bio-Sampler Impactors, S1.5.1.5). Sequences are deposited in the  
297 GenBank database under the following accession numbers: JX228219-JX228862.

298

### 299 ***S1.5.5 Freezing Tests***

300 Fungal and bacterial colonies (Andersen Cascade Bio-Sampler Impactor, S1.5.1.5) were picked  
301 and cultured in dextrose-peptone-yeast (DPY) medium (dextrose 10 g/L, peptone 3 g/L, yeast  
302 extract 0.3g/L) in 96-well polypropylene plates and incubated at 16 °C. A 50 µl aliquot of the  
303 inoculated DPY medium containing hyphal fragments and fungal spores was tested from each

304 well for its ice nucleation activity in a temperature range -12 °C to -2 °C. Aliquots were  
305 transferred to a fresh, sterile, 96-well polypropylene PCR tray and these were cooled in a thermal  
306 cycler (MJ Research, PTC-200). Temperature variation across the head was  $\pm 0.2$  °C of the true  
307 temperature measured using a thermistor (Bio-Rad, VPT-0300). The cycler was programmed to  
308 descend in 0.5 or 1 °C increments to -9.0 °C (the limit of the machine). After a 5 min dwell time  
309 at each temperature, the number of frozen wells was counted and the temperature lowered to the  
310 next level. Once at -9 °C, the tray was transferred to a 96-well aluminum incubation block  
311 (VWR, 13259-260) which had been pre-cooled to  $\sim -12$  °C inside a foam box in a freezer. The  
312 thermistor was inserted into a side well and after 10 min the block temperature and number of  
313 frozen wells was recorded. Aliquots of un-inoculated DPY medium were used as negative  
314 controls. Ice active isolates were then cultured on DPY agar and incubated at RT for  $\sim 3$  days.  
315 Beside microscopic analysis as described under S1.5.2 hyphal fragments and spores were picked  
316 into 20  $\mu$ l water, lysed at 95 °C for 10 min, and identified by DNA analysis as described above.

317

### 318 ***S1.6 Microscopic IN Activation Experiments***

319 Particles were collected on hydrophobic glass slides with a rotating MOUDI, as described above.  
320 The freezing properties of particles collected on the slides were then determined with an optical  
321 microscope and a flow cell with temperature and relative humidity control. The flow cell and  
322 microscope set-up was very similar to the ones used by Iannone et al. (2011) and Dymarska et al.  
323 (2006), to determine the ice nucleation properties of fungal spores and soot particles,  
324 respectively.

325

326 In every IN activation experiment, a hydrophobic slide containing particles was located within  
 327 the flow cell. The RH was first set to > 100% to condense water droplets on the particles. The  
 328 droplets were grown to approximately 100 μm in diameter, and after droplet growth was  
 329 completed each droplet contained between 30 and 100 particles. Next, the temperature was  
 330 decreased at a rate of 10 K/min until a temperature of -40 °C was reached. During the  
 331 experiment, between 11 and 66 droplets (average 36) were continuously monitored with an  
 332 optical microscope coupled to a CCD camera. From the images recorded with the CCD camera,  
 333 the freezing temperatures of the droplets were determined.

334  
 335 The number of ice nuclei in a freezing experiment,  $\#IN(T)$ , was calculated from the freezing data  
 336 using the following equation (Vali, 1971):

$$\text{Equation S2} \quad \#IN(T) = -\ln\left(\frac{N_{Total} - N_{Frozen}(T)}{N_{Total}}\right) \times N_{Total}$$

337  
 338 where  $N_{Total}$  is the total number of droplets in a freezing experiment and  $N_{Frozen}(T)$  is the number  
 339 of frozen droplets as a function of temperature in a freezing experiment. Equation S2 accounts  
 340 for the fact that multiple IN can exist in the same droplet (Vali, 1971). The number of ice nuclei  
 341 per volume of air as a function of temperature,  $[IN(T)]$ , was calculated using the following  
 342 equation:  
 343

$$\text{Equation S3} \quad [IN(T)] = \frac{\#IN(T)}{VolumeAirSampled} \times \frac{Area_{MOUDIStage}}{Area_{Monitored}}$$

344  
 345 where  $VolumeAirSampled$  is the total volume of air sampled by the MOUDI,  $Area_{MOUDIStage}$  is  
 346 the total area covered by particles within a MOUDI stage and  $Area_{Monitored}$  is the area  
 347 monitored with the microscope.

348

349 In the freezing experiments, a majority of the droplets froze by immersion freezing while a  
350 minority froze by contact freezing. Here immersion freezing refers to freezing of droplets by ice  
351 nuclei immersed in the liquid droplets, and contact freezing refers to freezing of liquid droplets  
352 by contact with neighboring frozen droplets (frozen droplets can grow by vapor transfer and  
353 eventually can come in contact with their neighbors). Droplets that froze by contact freezing  
354 were not considered when determining  $N_{Total}$  and  $N_{Frozen}(T)$  from the freezing data. In addition to  
355 immersion freezing and contact freezing, deposition freezing occasionally occurred in the  
356 freezing experiments. Here deposition freezing refers to freezing on a particle not immersed in a  
357 solution droplet. Deposition freezing was included in the calculations of  $[IN(T)]$  by adding the  
358 number of deposition freezing events to  $\#IN(T)$  calculated with Equation S2 above.

359  
360 Depending on the experimental conditions, the maximum concentration of ice nuclei,  $[IN(T)]$ ,  
361 that can be detected for any given slide (i.e. size interval sampled with the MOUDI) with the  
362 microscope freezing technique is roughly 0.6-0.9 L<sup>-1</sup> depending on the number of droplets  
363 condensed in an experiment and the total volume of air sampled by the MOUDI. As a result the  
364 maximum concentration of IN determined by the microscope technique is small compared to the  
365 maximum concentration determined with the CFDC method mentioned below.

366

367 ***S1.7 Real-Time Ice Nucleation Measurements with CFDC***

368 ***S1.7.1 IN Measurements***

369 A ground-based version of the Colorado State University continuous flow diffusion chamber  
370 (CFDC) (Rogers et al., 2001) was employed for real-time measurements of IN concentrations.  
371 The CFDC permits observation of ice formation on a continuous stream of particles at controlled

372 temperatures and humidities. In the CFDC, sampled air is directed vertically between two  
373 concentric ice-coated cylinders held at different temperatures, creating a zone supersaturated  
374 with respect to ice in the annular region. The sample air, ~15% of the total flow, is injected  
375 between two particle-free sheath flows. As the particles in the sample flow are exposed to ice  
376 supersaturations for several seconds, those particles active as IN under the sample temperature  
377 and humidity conditions are nucleated and grown to ice crystals larger than a few  $\mu\text{m}$  in size.  
378 These larger particles are distinguished from small non-IN aerosols by an optical particle counter  
379 (OPC) at the outlet of the instrument. Physical impaction of larger aerosols ( $>2.4 \mu\text{m}$ ) in advance  
380 of the CFDC and reduction of humidity conditions to ice saturation in the lower third of the  
381 chamber prevent false detection of large CN or cloud drops as ice nuclei. Temperatures ( $\pm 1^\circ\text{C}$ )  
382 and humidities ( $\pm 3\%$  RH with respect to water maximum uncertainty at  $-30^\circ\text{C}$ ) are well  
383 controlled in the instrument. For data used in this study, measurements were made at  $-25^\circ\text{C}$  at  
384 relative humidity in the range of 103% to 106%. Under these conditions, the CFDC directly  
385 measures IN activating by condensation/immersion freezing, and contributions are expected to  
386 the IN population from both dust and biological particles (Prenni et al., 2009). For the data in  
387 Figures 2E and 2F, particle concentrations were enhanced upstream using an MSP Corporation  
388 (Model 4240) aerosol concentrator. Measurements made using the concentrator were corrected to  
389 ambient concentrations based on the manufacturer's specifications for  $1 \mu\text{m}$  particles, corrected  
390 slightly for the sampling conditions at Manitou, as determined from direct measurements made  
391 approximately every other day. IN number concentrations are reported at standard temperature  
392 and pressure (STP; 1 atm and  $0^\circ\text{C}$ ).

393

394 CFDC measurements were collected at the following times are shown in Figures 2E and 2F E-F  
395 and discussed in the manuscript:

396	C01 (rain period)	8/2 10:27 – 17:57	(450 min.)
397	C02 (dry period)	8/17 16:27 – 23:47	(440 min.)

398  
399 Periods C01 and C02 correspond to sub-periods during MOUDI samples M10 and M27,  
400 respectively.

401

### 402 ***S1.7.2 DNA Analysis of IN Samples***

403 Ice crystals activated as IN in the CFDC were collected via impaction at the CFDC outlet (Prenni  
404 et al., 2009; Garcia et al., 2012). Residual IN were impacted onto a glass slide, which was coated  
405 with 5 mL of molecular grade mineral oil (Bio-Rad). DNA was then enzymatically extracted  
406 using Proteinase K. The extracted DNA was PCR amplified using the universal 515F and 1391R  
407 primers. The presence of biological IN was determined after PCR amplification via acrylamide  
408 gel electrophoresis. PCR products were cloned into a plasmid vector using the TOPO TA  
409 Cloning Kit® for sequencing (Invitrogen). Each clone was sequenced (Sanger method) and  
410 identified via Blast search against the National Center for Biotechnology Information (NCBI)  
411 genome database (2).

412 **References:**

- 413 Bozlee, B. J., Misra, A. K., Sharma, S. K. and Ingram, M.: Remote Raman and fluorescence  
414 studies of mineral samples, *Spectrochimica Acta Part a-Molecular and Biomolecular*  
415 *Spectroscopy*, 61, 2342-2348, 10.1016/j.saa.2005.02.033, 2005.
- 416 Després, V. R., Nowoisky, J. F., Klose, M., Conrad, R., Andreae, M. O. and Pöschl, U.:  
417 Characterization of primary biogenic aerosol particles in urban, rural, and high-alpine air by  
418 DNA sequence and restriction fragment analysis of ribosomal RNA genes, *Biogeosciences*, 4,  
419 1127-1141, 2007.
- 420 Dymarska, M., Murray, B. J., Sun, L. M., Eastwood, M. L., Knopf, D. A. and Bertram, A. K.:  
421 Deposition ice nucleation on soot at temperatures relevant for the lower troposphere, *J. Geophys.*  
422 *Res.-Atmos.*, 111, 10.1029/2005jd006627, 2006.
- 423 Foot, V. E., Kaye, P. H., Stanley, W. R., Barrington, S. J., Gallagher, M. and Gabey, A.: Low-  
424 cost real-time multi-parameter bio-aerosol sensors, *Proceedings of the SPIE - The International*  
425 *Society for Optical Engineering*, 711601 (711612 pp.), 10.1117/12.800226, 2008.
- 426 Fröhlich-Nowoisky, J., Pickersgill, D. A., Després, V. R. and Pöschl, U.: High diversity of fungi  
427 in air particulate matter, *Proceedings of the National Academy of Sciences*, 106, 12814-12819,  
428 10.1073/pnas.0811003106, 2009.
- 429 Fröhlich-Nowoisky, J., Burrows, S. M., Xie, Z., Engling, G., Solomon, P. A., Fraser, M. P.,  
430 Mayol-Bracero, O. L., Artaxo, P., Begerow, D., Conrad, P. G., Andreae, M. O., Després, V. and  
431 Pöschl, U.: Biogeography in the air: fungal diversity over land and oceans, *Biogeosciences*, 9,  
432 1125-1136, 10.5194/bg-9-1125-2012, 2012.
- 433 Gabey, A. M., Gallagher, M. W., Whitehead, J., Dorsey, J. R., Kaye, P. H. and Stanley, W. R.:  
434 Measurements and comparison of primary biological aerosol above and below a tropical forest  
435 canopy using a dual channel fluorescence spectrometer, *Atmospheric Chemistry and Physics*, 10,  
436 4453-4466, 10.5194/acp-10-4453-2010, 2010.
- 437 Garcia, E., Hill, T. C. J., Prenni, A. J., DeMott, P. J., Franc, G. D. and Kreidenweis, S. M.:  
438 Biogenic ice nuclei in boundary layer air over two U.S. High Plains agricultural regions, *Journal*  
439 *of Geophysical Research*, In Review, 2012.
- 440 Huffman, J. A., Treutlein, B. and Pöschl, U.: Fluorescent biological aerosol particle  
441 concentrations and size distributions measured with an Ultraviolet Aerodynamic Particle Sizer  
442 (UV-APS) in Central Europe, *Atmospheric Chemistry and Physics*, 10, 3215-3233, 2010.
- 443 Iannone, R., Chernoff, D. I., Pringle, A., Martin, S. T. and Bertram, A. K.: The ice nucleation  
444 ability of one of the most abundant types of fungal spores found in the atmosphere, *Atmospheric*  
445 *Chemistry and Physics*, 11, 1191-1201, 10.5194/acp-11-1191-2011, 2011.
- 446 Kaye, P. H., Stanley, W. R., Hirst, E., Foot, E. V., Baxter, K. L. and Barrington, S. J.: Single  
447 particle multichannel bio-aerosol fluorescence sensor, *Optics Express*, 13, 3583-3593, 2005.
- 448 Lighthart, B. and Shaffer, B. T.: Airborne bacteria in the atmosphere surface layer: temporal  
449 distribution above a grass seed field, *Applied and Environmental Microbiology*, 61, 1492-1496,  
450 1995.

451 Lindemann, J., Constantinidou, H. A., Barchet, W. R. and Upper, C. D.: Plants as sources of  
452 airborne bacteria, including ice nucleation-active bacteria, *Applied and Environmental*  
453 *Microbiology*, 44, 1059-1063, 1982.

454 Madelin, T. M.: Fungal Aerosols - A Review, *Journal of Aerosol Science*, 25, 1405-1412,  
455 10.1016/0021-8502(94)90216-x, 1994.

456 Marple, V. A., Rubow, K. L. and Behm, S. M.: A microorifice uniform deposit impactor  
457 (MOUDI) - description, calibration, and use, *Aerosol Sci. Technol.*, 14, 434-446,  
458 10.1080/02786829108959504, 1991.

459 Nikolcheva, L. G. and Bärlocher, F.: Taxon-specific fungal primers reveal unexpectedly high  
460 diversity during leaf decomposition in a stream, *Mycological Progress*, 3, 41-49, 2004.

461 Pöhlker, C., Huffman, J. A. and Pöschl, U.: Autofluorescence of atmospheric bioaerosols -  
462 fluorescent biomolecules and potential interferences, *Atmospheric Measurement Techniques*, 5,  
463 37-71, 10.5194/amt-5-37-2012, 2012.

464 Pöschl, U., Martin, S. T., Sinha, B., Chen, Q., Gunthe, S. S., Huffman, J. A., Borrmann, S.,  
465 Farmer, D. K., Garland, R. M., Helas, G., Jimenez, J. L., King, S. M., Manzi, A., Mikhailov, E.,  
466 Pauliquevis, T., Petters, M. D., Prenni, A. J., Roldin, P., Rose, D., Schneider, J., Su, H., Zorn, S.  
467 R., Artaxo, P. and Andreae, M. O.: Rainforest Aerosols as Biogenic Nuclei of Clouds and  
468 Precipitation in the Amazon, *Science*, 329, 1513-1516, 10.1126/science.1191056, 2010.

469 Prenni, A. J., Petters, M. D., Kreidenweis, S. M., Heald, C. L., Martin, S. T., Artaxo, P., Garland,  
470 R. M., Wollny, A. G. and Pöschl, U.: Relative roles of biogenic emissions and Saharan dust as  
471 ice nuclei in the Amazon basin, *Nature Geoscience*, 2, 402-405, 10.1038/ngeo517, 2009.

472 Robinson, N. H., Newton, H. M., Allan, J. D., Irwin, M., Hamilton, J. F., Flynn, M., Bower, K.  
473 N., Williams, P. I., Mills, G., Reeves, C. E., McFiggans, G. and Coe, H.: Source attribution of  
474 Bornean air masses by back trajectory analysis during the OP3 project, *Atmospheric Chemistry*  
475 *and Physics*, 11, 9605-9630, 10.5194/acp-11-9605-2011, 2011.

476 Rogers, D. C., DeMott, P. J., Kreidenweis, S. M. and Chen, Y.: A continuous-flow diffusion  
477 chamber for airborne measurements of ice nuclei, *J. Atmos. Ocean. Tech.*, 18, 725-741, 2001.

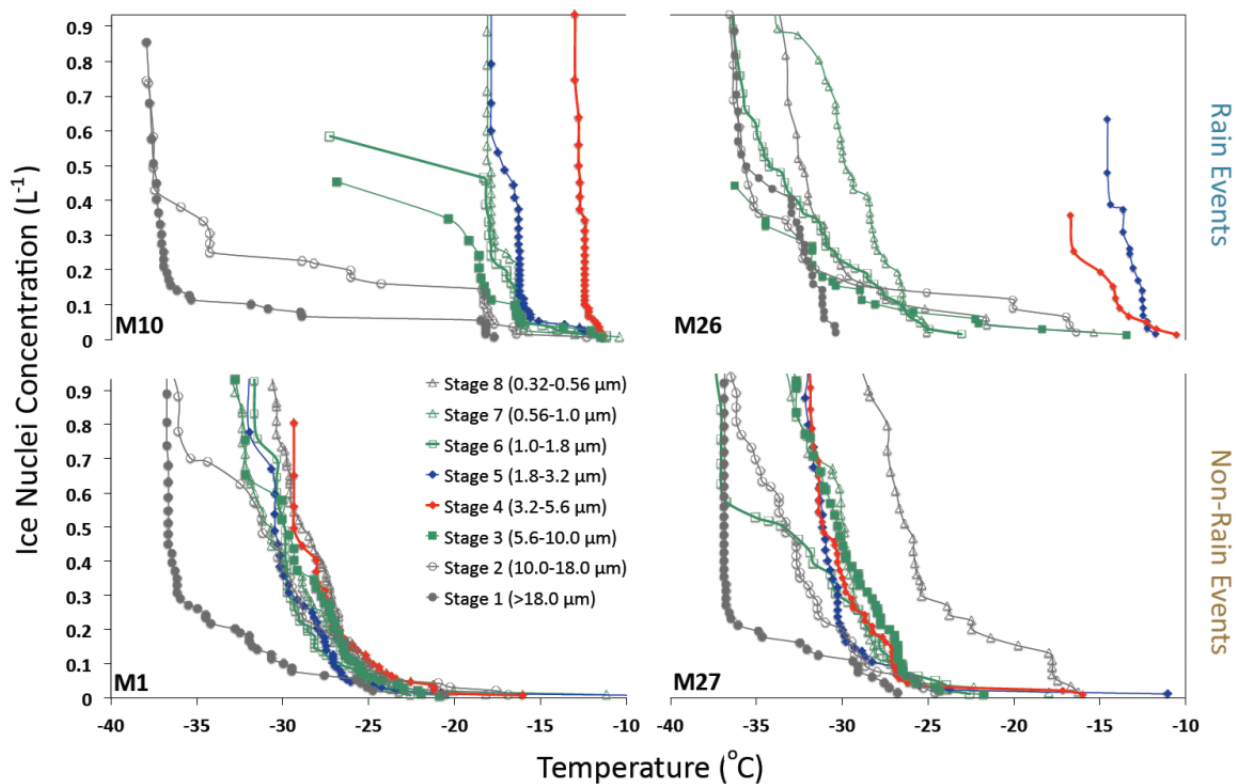
478 Sinha, B. W., Hoppe, P., Huth, J., Foley, S. and Andreae, M. O.: Sulphur isotope analysis of  
479 individual aerosol particles in the urban aerosol at a Central European site (Mainz, Germany),  
480 *Atmospheric Chemistry and Physics*, 8, 7217-7238, 2008.

481 Vali, G.: Quantitative evaluation of experimental results on heterogeneous freezing of  
482 supercooled liquids, *Journal of the Atmospheric Sciences*, 28, 402-&, 10.1175/1520-  
483 0469(1971)028<0402:qeoera>2.0.co;2, 1971.

484 Weisburg, W. G., Barns, S. M., Pelletier, D. A. and Lane, D. J.: 16S ribosomal DNA  
485 amplification for phylogenetic study, *J. Bacteriol.*, 173, 697-703, 1991.

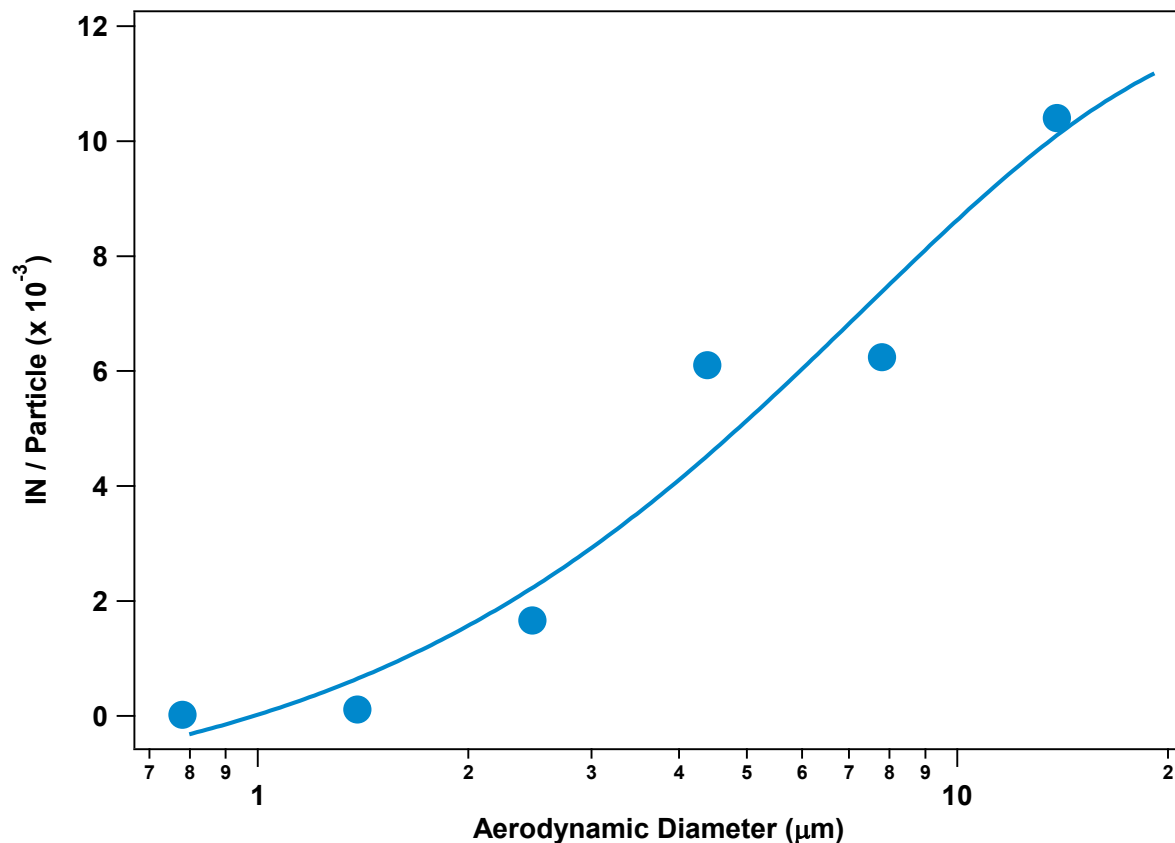
486 White, T. J., Bruns, T., Lee, S. and Taylor, J.: Amplification and Direct Sequencing of Fungal  
487 Ribosomal RNA genes for Phylogenetics, in: *PCR Protocols: a Guide to Methods and*  
488 *Applications*, edited by: Innis, M. A., Gelfand, D. H., Sninsky, J. J. and White, T. J., Academic  
489 Press, Inc., New York, 315-322, 1990.

490



491  
 492  
 493  
 494  
 495  
 496  
 497

**Figure S1:** IN activation curves from microscopic IN activation experiments with size-resolved aerosol samples (MOUDI stages). Upper panels (A,B) for samples collected during rain events, and lower panels (C,D) for samples collected during dry periods. Red traces show Stage 4 (3.2 – 5.6  $\mu\text{m}$ ), blue traces show Stage 5 (1.8 – 3.2  $\mu\text{m}$ ), and light green traces show Stage 3, 6, 7 (5.6-10, 1.0-1.8, and 0.56-1.0  $\mu\text{m}$ , respectively). See SOM section S1.5.1.1 for sampling dates.



498  
 499  
 500 **Figure S2:** An estimate of the fraction of particles collected during rain events (M10, M26) that can serve as IN at  
 501 -15 °C. IN concentrations were calculated from microscopic IN activation experiments and particle concentrations  
 502 were calculated from UV-APS measurements. See SOM section S1.5.1.1 for sampling dates. Note that the fraction  
 503 of particles with IN activity is greater than 1 in 1000 for all particles >2 μm and exceeds 1 in 100 for particles >10  
 504 μm. Exponential curve shown to guide the eye.